ROYAL SOCIETY
OF CHEMISTRY

PAPER

New near-infrared absorbing conjugated electron donor–acceptor molecules with a fused tetrathiafulvalene–naphthalene diimide framework†

Qi Zhou,[ab] Junfang Yang,[b] Mingxu Du,[a] Xiaobo Yu,[ab] Cheng Li, [ID][ab] Xi-Sha Zhang,[ab] Qian Peng,[b] Guanxin Zhang [ID]*[ab] and Deqing Zhang [ID]*[ab]

Molecular materials that can absorb and emit light in the near-infrared (NIR) region are attracting more and more attention in many fields. In this paper, we report the synthesis and studies of the photophysical and semiconducting properties of tetrathiafulvalene (TTF)–naphthalene diimide (NDI) fused molecules (**NDITTF2**, **NDI2TTF** and **NDI2TTF3**). The results reveal that all molecules show strong absorptions in the NIR region, and their absorption maxima can reach 1015 nm with molar extinction coefficients (ε) up to 66 900 M^{-1} cm^{-1} in the solution state. Moreover, NIR emissions were found for **NDITTF2** and **NDI2TTF** either in solution or in the film state. The emission maxima in the $CHCl_3$ solution locate at 892 nm for **NDI2TTF** (ϕ = 1.64%) and 1062 nm for **NDITTF2** (ϕ = 0.21%). Furthermore, the thin film of **NDITTF2** was found to show p-type semiconducting properties with a hole mobility up to 0.45 cm^2 V^{-1} s^{-1}.

1. Introduction

Organic molecules that can absorb and emit light in the near-infrared (NIR, > 750 nm) region are of tremendous interest because of their practical applications in a number of important fields, such as organic photovoltaics, NIR light photodetectors, bioimaging, phototherapy, *etc.*[1–12] Due to the fact that NIR light exhibits low light scattering and deep penetration behaviors and most biological samples absorb weakly in the NIR region which can lower the background absorbance and autofluorescence, these NIR-absorbing and emitting molecules are particularly interesting for photodiagnosis (*e.g.* NIR fluorescence imaging and photoacoustic imaging) and phototherapy (*e.g.* photodynamic therapy and photothermal therapy).[9–12] To meet the urgent demand for NIR absorbing and emitting materials, various design approaches have been adopted, such as extension of the conjugation length, reduction of bond length alternation, and introduction of appropriate electron donor and acceptor units.[1,2] Among them, introduction of a strong electron donor (D) and a strong electron acceptor (A) in

small molecules and polymers becomes a common strategy to realize such materials.

As a typical strong electron donor, tetrathiafulvalene (TTF) and its derivatives have played a key role in the construction of organic conductors and superconductors in the past several decades.[13,14] With the passage of time, abundant properties of TTF have been exploited, which made them intensively studied in many fields including chemical sensors, molecular devices as well as optoelectronic devices in the recent years.[15–29] Among these TTF derivatives, TTF based conjugated electron donor–acceptor systems have received extensive attention. This is because the incorporation of TTF units in a conjugated way can raise the highest occupied molecular orbital (HOMO) energy levels of the D–A molecules, redshift the absorption and enhance the intermolecular interaction.[23] Such modifications can enrich the physical and chemical properties of TTF derivatives and thus enable them to be applied in organic optoelectronic materials. Up to now, all kinds of TTF based electron donor–acceptor systems had been developed.[13–29] However, TTF-based molecules with both NIR-absorbing and emitting properties remain scarcely reported.

Herein, we report three D–A molecules: **NDITTF2**, **NDI2TTF** and **NDI2TTF3** (see Scheme 1), in which the TTF and naphthalene diimide (NDI) moieties are fused in conjugated ways. The combinations of both strong electron donating and accepting units are likely to redshift their absorptions to the NIR region. In addition, the fusion of TTF with NDI units might endow them with not only NIR absorption but also NIR emission

a Beijing National Laboratory for Molecular Sciences, CAS Key Laboratories of Organic Solids, CAS Research/Education Center for Excellence in Molecular Sciences, Institute of Chemistry, Chinese Academy of Sciences, Beijing, 100190, P. R. China. E-mail: dqzhang@iccas.ac.cn, gxzhang@iccas.ac.cn

b University of Chinese Academy of Sciences, Beijing 100049, P. R. China

† Electronic supplementary information (ESI) available. See DOI: 10.1039/d1tc04291b

Scheme 1 Chemical structures of **NDI-1**, **NDITTF2**, **NDI2TTF** and **NDI2TTF3** and the synthetic approach.

Fig. 1 Absorption spectra of chloroform solutions (solid lines) and thin films (dashed lines) of **NDITTF2**, **NDI2TTF** and **NDI2TTF3**. The concentration for each molecule was 10 μM.

properties.[23,27–29] The results manifest that **NDITTF2**, **NDI2TTF** and **NDI2TTF3** exhibit NIR absorptions and the maximum absorption of **NDI2TTF3** in the film state can reach 1072 nm. Moreover, emissions in solution were detected for **NDITTF2** and **NDI2TTF**. The maximum emissions of $CHCl_3$ solutions of **NDITTF2** and **NDI2TTF** appear around 1062 and 892 nm, with quantum yields of 0.21% and 1.64%, respectively. Finally, thin-film OFETs based on **NDITTF2** exhibit good a hole mobility up to 0.45 cm^2 V^{-1} s^{-1}.

2. Results and discussion

Synthesis and characterization

As shown in Scheme 1, the reaction of NDIBr4 with potassium O-t-butyl dithiocarbonate afforded the key intermediate (**NDI-1**) in 71.5% yield, which can be transformed into **NDITTF2** in 68.2% yield after reaction with 5-bis-(methylthio)-1,3-dithiole-2-thione. Meanwhile, self-coupling of **NDI-1** in the presence of triethylphosphite formed **NDI2TTF** in 45.3% yield, which further reacted with 4,5-bis(hexylthio)-1,3-dithiole-2-thione to form **NDI2TTF3** in 19.1% yield. All the reactions were carried under a nitrogen atmosphere. **NDITTF2**, **NDI2TTF** and **NDI2TTF3** were characterized by NMR and high-resolution mass spectrometry (HRMS) as well as elemental analysis. Also, as shown in Fig. S1 (ESI†), the degradation temperatures at 5% weight loss were measured to be 348 °C for **NDITTF2**, 426 °C for **NDI2TTF** and 311 °C for **NDI2TTF3**, indicating that they all show good thermal stability.

Spectroscopic studies and theoretical calculations

The UV-vis absorption spectra of **NDITTF2**, **NDI2TTF** and **NDI2TTF3** in chloroform are shown in Fig. 1 and the respective absorption peaks are collected in Table 1. Intense broad absorptions in the region of 500–1200 nm were detected for **NDI2TTF**, **NDITTF2** and **NDI2TTF3**. Moreover, these absorptions are red-shifted in the following order: **NDI2TTF** < **NDITTF2** < **NDI2TTF3**. The absorptions of the thin films of

NDITTF2, **NDI2TTF** and **NDI2TTF3** were also measured. As shown in Fig. 1, the absorption spectra of the thin films of **NDITTF2**, **NDI2TTF** and **NDI2TTF3** were all red-shifted compared to those in solutions owing to the intermolecular interactions within their thin films, which may involve intermolecular electron donor and acceptor interactions. Based on the absorption edges of their thin films, the band gaps of **NDITTF2**, **NDI2TTF** and **NDI2TTF3** were estimated to be 1.03 eV, 1.09 eV and 0.99 eV, respectively. These are in good agreement with those obtained with cyclic voltammetry data as it will be discussed below.

Density functional theory (DFT) and time-dependent DFT (TDDFT) calculations were performed to figure out the origin of the absorption spectra of the three compounds by using the B3LYP functional and the 6-31G(d) basis set. Briefly, the calculated results are given in Fig. S2, S3 and Tables S1–S3 (ESI†), including the absorption peak positions, oscillator strengths, transition properties and the charge density of the frontier molecular orbitals. Comparing the calculated and experimental results, it can be inferred that (i) the absorptions are red-shifted gradually from **NDI2TTF** through **NDITTF2** to **NDI2TTF3**, in good agreement with the respective absorption spectra measured experimentally (see Fig. S3, ESI†); (ii) the absorptions in the long-wavelength regions mainly stem from the transition from S_0 to S_1 with large oscillator strength for the three compounds, which agrees with the strong absorption intensity observed in the experimental spectra. The fine structures may be caused by the contribution from vibration structures, which are very common in rigid organic compounds.[30] The maximum absorption for **NDI2TTF3** deviates from the 0–0 transition and blue-shifted to 915 nm owing to the vibration-caused satellite band, which results in the difference between the experimental value and the calculated one without considering the vibration effect. The electronic transition and orbital properties indicate that **NDITTF2** and **NDI2TTF3** have similar features: the transition is mainly from the HOMO to the LUMO, and the HOMO is delocalized over TTF and the naphthalene ring of NDI and the LUMO is largely concentrated

This journal is © The Royal Society of Chemistry 2022

J. Mater. Chem. C, 2022, **10**, 2814–2820 | **2815**

Table 1 The absorption and fluorescence data, HOMO/LUMO energies and bandgaps of **NDITTF2**, **NDI2TTF** and **NDI2TTF3**

Compd	λ^a (nm)		λ^d (nm)			E_{LUMO} (eV)	E_{HOMO}^f (eV)	$E_g^{cv\,g}$ (eV)	$E_g^{opt\,h}$ (eV)
	Solution^b (ε, M^{-1} cm^{-1})	Film^c (α, cm^{-1})	Solution	Film	Φ^e (%)				
NDITTF2	946 (42 900), 858 (31 600), 439, 413	1052 (165 000), 892 (176 000)	1062	1188	0.21	−3.60	−4.96	1.36	1.03
NDI2TTF	846 (66 900), 765 (60 500), 444, 421	872 (166 000), 790 (161 000)	892, 1005	1158	1.64	−4.12	−5.54	1.42	1.09
NDI2TTF3	1015 (40 400), 915 (47 800), 448, 413	1072 (173 000), 915(154 000)	—	—	—	−3.64	−4.93	1.29	0.99

^{a} Absorption peaks in CHCl$_3$ solution (1.0 × 10^{-5} M) and spin-coated thin films. ^{b} Molar extinction coefficient. ^{c} Extinction coefficient for spin-coated thin films. ^{d} Emission peaks in CHCl$_3$ solution (1.0 × 10^{-5} M) and spin-coated thin films. ^{e} Quantum yield in CHCl$_3$ solution (1.0 × 10^{-5} M). ^{f} Estimated using the equations: $E_{HOMO} = -(E_{ox1}^{1/2} + 4.8 - E_{ox}^{FcFc+})$ eV and $E_{LUMO} = -(E_{red1}^{1/2} + 4.8 - E_{ox}^{FcFc+})$ eV, where the $E_{ox1}^{1/2}$ and $E_{red1}^{1/2}$ values can be found in Table S4 (ESI), and $E_{ox}^{FcFc+} = 0.56$ V. ^{g} $E_g^{cv} = E_{LUMO} - E_{HOMO}$. ^{h} Calculated on the basis of the onset of thin film absorption spectra; '—' means too weak to be detected.

on the NDI moiety, which leads to a very similar absorption spectrum. At the same time, it suggests a bit stronger conjugation degree in **NDI2TTF3** than in **NDITTF2**, which results in a slight enhancement of the HOMO and the decrease of the LUMO in energy for **NDI2TTF3** by comparing **NDITTF2**; thus, it rationally explains the red-shift of the absorption bands. Differently, the absorption of **NDI2TTF** is caused by the transition between the HOMO and LUMO which both spread over the whole molecule, resulting in a blue-shifted absorption spectrum relative to **NDITTF2** and **NDI2TTF3**. (iii) The short-wavelength absorptions mainly come from S$_3$ (HOMO−2 → LUMO) and S$_5$ (HOMO−6 → LUMO and HOMO−3 → LUMO) for **NDITTF2**, S$_4$ (HOMO−2 → LUMO) and S$_7$ (HOMO−1 → LUMO+1) for **NDI2TTF** and S$_9$ (HOMO−4 → LUMO and HOMO−3 → LUMO) and S$_{10}$ (HOMO−3 → LUMO and HOMO−4 → LUMO) for **NDI2TTF3** (Table S1–S3, ESI†).

NIR fluorescence was detected for **NDITTF2** and **NDI2TTF** both in the solution state and in the film state (see Fig. 2). For example, the emission maxima locate at 892 nm for **NDI2TTF** and 1062 nm for **NDITTF2** after being excited with an 808 nm light source, and their quantum yields were 1.64% and 0.21%, respectively (see Table 1). Compared with their solution fluorescence spectra, large red-shifted emissions up to 1188 and 1158 nm were observed for thin films of **NDITTF2** and **NDI2TTF** (see Fig. 2), respectively, though their quantum yields were too
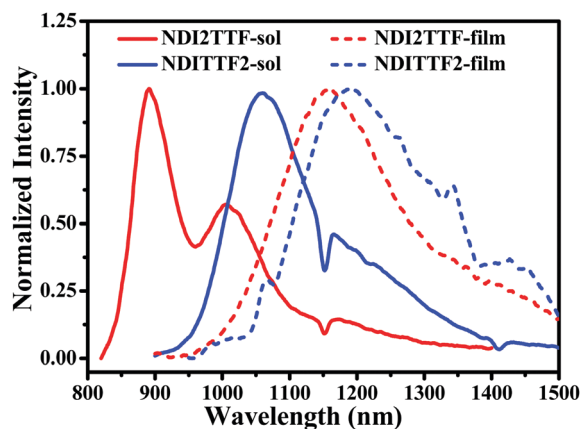
low to be detected. But almost no fluorescence was detected for **NDI2TTF3** in both solution and thin film states.

It is well known that the absorption and emission spectra of D–A molecules show solvatochromic behavior. Fig. S4 and S5 (ESI†) show the absorption of **NDITTF2**, **NDI2TTF** and **NDI2TTF3** and emission spectra of **NDITTF2** and **NDI2TTF** in chloroform, chlorobenzene and toluene with different polarities. Redshifts (albeit slight) of both absorption and emission spectra of these molecules were observed by increasing the solvent polarities. This indicates the existence of charge transfer character in these molecules.[25–27]

Electrochemical and spectroelectrochemical studies

Cyclic voltammograms (CVs) and differential pulse voltammograms (DPVs) of **NDITTF2**, **NDI2TTF** and **NDI2TTF3** were measured (see Fig. 3) by using a ferrocene/ferrocenium (Fc/Fc+) redox couple as the reference standard (see Fig. S6, ESI†), and the respective oxidation and reduction potentials are presented in Table S4 (ESI†). As shown in Fig. 3, all the three molecules show multistate redox properties. For example, **NDITTF2** undergoes six reversible redox processes ($E_{ox1}^{1/2}$ = 0.72 V, $E_{ox2}^{1/2}$ = 0.96 V, $E_{ox3}^{1/2}$ = 1.30 V, $E_{ox4}^{1/2}$ = 1.43 V, $E_{red1}^{1/2}$ = −0.64 V, $E_{red2}^{1/2}$ = −1.01 V), which can be assigned to the oxidation of the TTF units and the reduction of the NDI moiety. **NDI2TTF** and **NDI2TTF3** also exhibit quasi-reversible redox waves. As compared to those of **NDI2TTF3** ($E_{ox1}^{1/2}$ = 0.69 V, $E_{red1}^{1/2}$ = −0.60 V), the redox potentials ($E_{ox1}^{1/2}$ =1.3 V and $E_{red1}^{1/2}$ = −0.11 V) of **NDI2TTF** are positively shifted. This may be caused by the two electron withdrawing carbonyl groups in **NDI2TTF**.
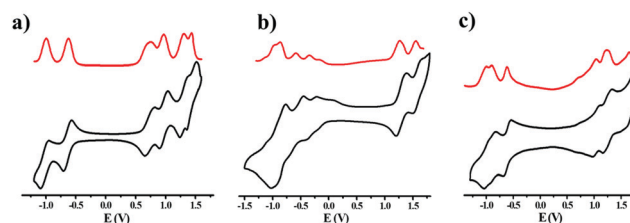

Fig. 2 Normalized emission spectra of the CHCl$_3$ solutions (solid lines) and thin films (dashed lines) of **NDITTF2** and **NDI2TTF**. The concentration for each molecule was 10 μM and the excitation wavelength was 808 nm.

Fig. 3 DPVs (red line) and CVs (black line) of **NDITTF2** (a), **NDI2TTF** (b) and **NDI2TTF3** (c) in a mixture of o-dichlorobenzene and CH$_2$Cl$_2$ (1 : 1, v/v) at a scan rate of 100 mV s^{-1} with a Pt disc (2 mm diameter) as the working electrode, a Pt wire as the counter electrode, a Ag wire as the reference electrode, and n-Bu$_4$NPF$_6$ (0.1 M) as the supporting electrolyte. The concentration of each sample was 1 mM.

2816 | *J. Mater. Chem. C*, 2022, **10**, 2814–2820

This journal is © The Royal Society of Chemistry 2022

Fig. 4 The transfer and output characteristics of the FET device based on **NDITTF2** after being annealed at 160 °C for 15 min. The transistor channel width and channel length were 1440 μm and 40 μm, respectively.

Fig. 5 XRD pattern of the as-cast thin-film of **NDITTF2** and that after annealing at 160 °C for 15 min.

The HOMO/LUMO energies were estimated to be $-4.96/-3.6$, $-5.54/-4.12$ and $-4.93/-3.64$ eV for **NDITTF2**, **NDI2TTF** and **NDI2TTF3**, respectively (see Table 1). Obviously, the HOMO energy increases in the following order: **NDI2TTF** < **NDITTF2** < **NDI2TTF3**, which agrees well with the order obtained from theoretical calculations (see Table S4, ESI†). The band gaps were estimated to be 1.36 eV, 1.42 eV and 1.29 eV for **NDITTF2**, **NDI2TTF** and **NDI2TTF3**, respectively, based on their HOMO/LUMO energies.

We also investigated the variation of the absorption spectrum upon electrochemical oxidation/reduction for **NDITTF2**. Oxidation of the dichlorobenzene/CH_2Cl_2 (1:1, v/v) solution of **NDITTF2** containing n-Bu$_4$NPF$_6$ (0.15 M) was performed by applying an oxidation potential of 0.8 V (*vs* Ag wire). Obviously, as shown in Fig. S7A (ESI†), a steady decrease in the absorption band around 918 nm and emergence of an absorption band around 1083 nm as well as a broad absorption from 2044 nm to 3075 nm were observed. This variation of the absorption spectra should be attributed to the transformation of neutral **NDITTF2** into its radical cation form. This was proved by chemical oxidation of **NDITTF2**. For example, as shown in Fig. S8 (ESI†), the absorption band around 1083 nm and the broad absorption from 2044 nm to 3075 nm appeared and reached their maxima after the addition of 2.66 eq. of Fe(ClO$_4$)$_3$. Interestingly, application of a reduction potential of 0.4 V (*vs.* Ag wire) to the solution to which an oxidation potential was applied for 2000 s resulted in a gradual decrease of the absorption band to around 1083 nm and the broad absorption from 2044 nm to 3075 nm (Fig. S7B, ESI†). After the electrochemical reduction was carried out for 500 s, the initial absorption spectrum of the solution was almost recovered. Briefly, the NIR absorption of **NDITTF2** can be reversibly modulated by the sequential electrochemical oxidation and reduction.

Thin film semiconducting properties

The semiconducting properties of **NDITTF2**, **NDI2TTF** and **NDI2TTF3** were explored by fabrication of top-gate/bottom-contact (TGBC) OFETs with their thin films on OTS (octadecyltrichlorosilane) modified SiO$_2$/Si substrates (see the ESI†).

Fig. 4 and Fig. S9 (ESI†) show the transfer and output curves for the FET with a thin film of **NDITTF2** before and after thermal annealing. Clearly, I_{DS} increases when applying a negative V_{Gs}, which means that **NDITTF2** exhibits p-type semiconducting behavior, agreeing well with its HOMO and LUMO energy levels as discussed above.[31] The average hole mobility of the as-prepared spin-coated thin film of **NDITTF2** was extracted to be 0.31 cm^2 V^{-1} s^{-1}. Further thermal annealing of the thin film of **NDITTF2** has no remarkable effect on the enhancement of mobility. For example, the maximum mobility can be boosted to only 0.45 cm^2 V^{-1} s^{-1} even after thermal annealing at 160 °C for 15 min (see Table S5, ESI†). However, the semiconducting properties of thin films of **NDI2TTF** and **NDI2TTF3** are too poor to be detected.

Thin films of **NDITTF2** before and after annealing were investigated with X-ray diffraction (XRD) and atomic force microscopy (AFM). As depicted in Fig. 5, two very weak diffraction peaks were detected for the thin-film of **NDITTF2** before annealing. After annealing at 160 °C for 15 min, the diffraction intensities of both peaks (3.37° and 6.75°) were slightly enhanced. These results reveal that the crystallinity of the thin film of **NDITTF2** is slightly enhanced after annealing. The AFM images of thin-films of **NDITTF2** before and after annealing were further recorded as depicted in Fig. S10 (ESI†). After annealing, the morphology of the thin film of **NDITTF2** was smoother and more uniform with a better continuity and the root-mean square roughness (R_{RMS}) values varied from 6.01 nm to 4.64 nm. Thus, the results of both XRD and AFM studies are in agreement with the fact that the hole mobility of the thin-film of **NDITTF2** can be enhanced slightly after annealing.

3. Conclusion

In summary, three TTF–NDI fused and conjugated D–A systems (**NDITTF2**, **NDI2TTF** and **NDI2TTF3**) were synthesized and studied. They all exhibit rigid and planar structures, and their HOMO orbitals are delocalized over their entire π system, while their LUMOs were mainly localized on the NDI fragments, based on the DFT calculations. They all show strong absorptions in the NIR region, and the absorption maximum for the thin film of **NDI2TTF3** can be extended to 1072 nm. Moreover, the CHCl$_3$ solutions of **NDITTF2** and **NDI2TTF** are emissive in

the NIR region with emission maxima at 1062 and 892 nm, with quantum yields of 0.21% and 1.64%, respectively. Furthermore, the thin film of **NDITTF2** was found to show p-type semiconducting properties with a hole mobility up to 0.45 cm^2 V^{-1} s^{-1}. Further structural modifications of these molecules are underway with the end to improve their quantum yields in the NIR region as well as explore their applications in photodiagnosis and phototherapy.

4. Experimental section

Synthesis of NDI-1

Under a nitrogen atmosphere, a mixture of NDIBr4 (2.5 g, 2 mmol) and potassium O-t-butyl dithiocarbonate (1.12 g, 6 mmol) in THF (100 mL) was stirred at 0 °C for 1 hour. After the reaction, the solvent was removed by rotary evaporation and the crude product was purified by silica gel chromatography with petroleum ether (60–90 °C) and CH$_2$Cl$_2$ (4:1, v/v) as the eluent to give **NDI-1** (1.59 g) as a yellow solid in 71.5% yield. ^{1}H NMR (300 MHz, CDCl$_3$) δ 4.19 (d, J = 7.2 Hz, 4H), 2.01 (br, 2H), 1.68–0.98 (m, 80H), 0.87 (t, J = 6.0 Hz, 12H). ^{13}C NMR (75 MHz, CDCl$_3$) δ 195.23, 162.16, 143.21, 123.75, 117.50, 46.04, 36.40, 31.94, 31.45, 30.01, 29.70, 29.66, 29.60, 29.38, 26.22, 22.71, 14.13. HRMS (MALDI-TOF): calcd for C$_{64}$H$_{98}$N$_2$O$_6$S$_4$, 1118.6313; found, 1118.6308. Elemental analysis: calcd for C$_{64}$H$_{98}$N$_2$O$_6$S$_4$: C 68.65, H 8.82, N 2.50; found: C 68.73, H 8.84, N 2.50.

Synthesis of NDITTF2

Under a nitrogen atmosphere, to a mixture of 4, 5-bis (methylthio)-1,3-dithiole-2-thione (204 mg, 0.9 mmol) and **NDI-1** (100 mg, 0.09 mmol) in a Schlenk tube, triethylphosphite (10 mL) was added. Then the mixture was stirred at 140 °C for 4 h. After being cooled to room temperature, the resulting mixture was poured into methanol (30 mL) and filtered. The residue was purified by silica gel chromatography with gradient elution: firstly, the mixture of petroleum ether (60–90 °C) and CH$_2$Cl$_2$ (4:1, v/v) was used to remove the impurities, then CHCl$_3$ was used to wash the product out of the silica gel column. Finally, **NDITTF2** (0.091 g) was obtained in 68.2% yield. ^{1}H NMR (500 MHz, CDCl$_2$) δ 4.18 (d, J = 6.9 Hz, 4H), 2.52 (s, 12H), 2.12 (br, 2H), 1.61–1.01 (m, 80H), 0.89–0.87 (br, 12H). ^{13}C NMR (125 MHz, o-dichlorobenzene-d4) δ 162.39, 147.88, 128.09, 125.71, 116.81, 115.57, 114.02, 46.18, 37.15, 32.39, 32.01, 30.48, 29.88, 29.43, 26.90, 22.70, 18.71, 13.92. HRMS (MALDI-TOF): calcd for C$_{74}$H$_{110}$N$_2$O$_4$S$_{12}$, 1474.5109; found, 1474.5101. Elemental analysis: calcd for C$_{74}$H$_{110}$N$_2$O$_4$S$_{12}$: C 60.20, H 7.51, N 1.90; found: C 60.16, H 7.53, N 1.92.

Synthesis of NDI2TTF

Under a nitrogen atmosphere, a toluene solution of **NDI-1** (800 mg, 0.7 mmol) and triethylphosphite (1.0 mL) was stirred at 100 °C for one hour. After being cooled to room temperature, the resulting mixture was poured into methanol (30 mL) and filtered, and the residue was purified by silica gel chromatography

with petroleum ether (60–90 °C) and CH$_2$Cl$_2$ (4:1, v/v) to give **NDI2TTF** (0.35 g, 45.3%). ^{1}H NMR (500 MHz, CDCl$_2$) δ 4.30 (d, J = 6.5 Hz, 8H), 2.18 (br, 4H), 1.94–1.01 (m, 160H), 0.89–0.87 (br, 24H); ^{13}C NMR (126 MHz, toluene-$d8$) δ 193.38, 162.11, 162.02, 148.15, 140.95, 124.85, 122.99, 117.27, 115.14, 46.67, 36.93, 32.35, 31.87, 30.43, 29.84, 29.70, 29.65, 29.33, 29.27, 26.91, 22.50, 13.54; HRMS (MALDI-TOF): calcd for C$_{128}$H$_{196}$N$_4$O$_{10}$S$_8$, 2205.2723; found, 2205.2747. Elemental analysis for C$_{128}$H$_{196}$N$_4$O$_{10}$S$_8$: C 69.65, H 8.95, N 2.54; found: C 69.62, H 8.96, N 2.39.

Synthesis of NDI2TTF3

Under a nitrogen atmosphere, a toluene solution of **NDI2TTF** (100 mg, 0.046 mmol), 4,5-bis(hexylthio)-1,3-dithiole-2-thione (366 mg, 1 mmol) and triethylphosphite (1.0 mL) was stirred at 120 °C for 12 hours. After being cooled to room temperature, the resulting mixture was poured into methanol (30 mL) and filtered. The residue was purified by silica gel chromatography with gradient elution: firstly, the mixture of petroleum ether (60–90 °C) and CH$_2$Cl$_2$ (4:1, v/v) and CH$_2$Cl$_2$ were used to remove the impurities sequentially; then CHCl$_3$ was used to wash the product out of the silica gel column. Finally, **NDI2TTF3** (0.025 g) was obtained in 19.1% yield. ^{1}H NMR (500 MHz, C$_6$D$_4$Cl$_2$) δ 4.54 (br, 8H), 3.08 (br, 8H), 2.60 (br, 4H), 2.28–1.13 (m, 192H), 1.03 (br, 36H). ^{13}C NMR (100 MHz, solid) δ 161.44, 146.61, 124.91, 113.64, 46.54, 36.20, 30.65, 23.53, 14.77. HRMS (MALDI-TOF): calcd for C$_{158}$H$_{248}$N$_4$O$_8$S$_{16}$, 2841.4648; found, 2841.4667. Elemental analysis: calcd for C$_{142}$H$_{216}$N$_4$O$_{10}$S$_{16}$: C 66.71; H 8.79, N 1.97, found: C 67.01, H 8.76, N 1.91.

Conflicts of interest

There are no conflicts to declare.

Acknowledgements

Notes and references

1 Z. Wang, *Near-Infrared Organic Materials and Emerging Application*, CRC Press, New York, 2013.
2 (*a*) J. Fabian, H. Nakazumi and M. Matsuoka, *Chem. Rev.*, 1992, **92**, 1197; (*b*) J. Qi, W. Qiao and Z. Wang, *Chem. Rec.*, 2016, **16**, 1531; (*c*) G. Qian and Z. Y. Wang, *Chem. – Asian J.*, 2010, **5**, 1006.
3 (*a*) C. Liu, K. Wang, X. Gong and A. J. Heeger, *Chem. Soc. Rev.*, 2016, **45**, 4825; (*b*) Z. Hu, J. Wang, X. Ma, J. Gao, C. Xu, K. Yang, Z. Wang, J. Zhang and F. Zhang, *Nano Energy*, 2020,

2818 | *J. Mater. Chem. C*, 2022, **10**, 2814–2820

This journal is © The Royal Society of Chemistry 2022

78, 105376; (*c*) Z. Zhang and Y. Li, *Angew. Chem., Int. Ed.*, 2021, **60**, 4422.

4 (*a*) D. Lim, J. Ha, H. Choi, S. C. Yoon, B. R. Lee and S. Ko, *Nanoscale Adv.*, 2021, **3**, 4306; (*b*) B. Xie, Z. Chen, L. Ying, F. Huang and Y. Cao, *InfoMat*, 2020, **2**, 57–91.

5 (*a*) S. Dai, T. Li, W. Wang, Y. Xiao, T. Lau, Z. Li, K. Liu and X. Zhan, *Adv. Mater.*, 2018, **30**, 1706571; (*b*) Y. Sun, Y. Zhang, Y. Ran, L. Shi, Q. Zhang, J. Chen, Q. Li, Y. Guo and Y. Liu, *J. Mater. Chem. C*, 2020, **8**, 15168; (*c*) Z. Xie, D. Liu, Y. Zhang, Q. Liu, H. Dong and W. Hu, *Chem. J. Chin. Univ.*, 2020, **41**, 1179.

6 (*a*) Z. Wu, Y. Zhai, H. Kim, J. D. Azoulay and T. N. Ng, *Acc. Chem. Res.*, 2018, **51**, 3144; (*b*) X. Liu, Y. Lin, Y. Liao, J. Wu and Y. Zheng, *J. Mater. Chem. C*, 2018, **6**, 3499; (*c*) N. Li, Z. Lan, L. Cai and F. Zhu, *J. Mater. Chem. C*, 2019, **7**, 3711.

7 X. Gong, M. Tong, Y. Xia, W. Cai, J. Moon, Y. Cao, G. Yu, C. Shieh, B. Nilsson and A. Heeger, *Science*, 2009, **325**, 1665.

8 (*a*) J. Kim, A. Liess, M. Stolte, A. Krause, V. Stepanenko, C. Zhong, D. Bialas, F. Spano and F. Würthner, *Adv. Mater.*, 2021, **33**, 2100582; (*b*) J. Huang, J. Lee, J. Vollbrecht, V. V. Brus, A. L. Dixon, D. Cao, Z. Zhu, Z. Du, H. Wang, K. Cho, G. C. Bazan and T. Nguyen, *Adv. Mater.*, 2020, **32**, 1906027; (*c*) S. Anantharaman, K. Strassel, M. Diethelm, A. Gubicza, E. Hack, R. Hany, F. Nüesch and J. Heier, *J. Mater. Chem.*, 2019, **7**, 14639.

9 (*a*) S. He, J. Song, J. Qu and Z. Cheng, *Chem. Soc. Rev.*, 2018, **47**, 4258; (*b*) Z. Guo, S. Park, J. Yoon and I. Shin, *Chem. Soc. Rev.*, 2014, **43**, 16; (*c*) C. Yan, Y. Zhang and Z. Guo, *Coord. Chem. Rev.*, 2021, **427**, 213556; (*d*) J. Li and K. Pu, *Chem. Soc. Rev.*, 2019, **48**, 38; (*e*) H. Kobayashi and P. L. Choyke, *Acc. Chem. Res.*, 2019, **52**, 2332.

10 (*a*) Y. Su, B. Yu, S. Wang, H. Cong and Y. Shen, *Biomaterials*, 2021, **271**, 120717; (*b*) P. Liu, X. Mu, X. Zhang and D. Ming, *Bioconjugate Chem.*, 2020, **31**, 260; (*c*) P. Reineck and B. C. Gibson, *Adv. Opt. Mater.*, 2017, **5**, 1600446.

11 (*a*) K. Pu, J. Mei, J. Jokerst, G. Hong, A. Antaris, N. Chattopadhyay, A. Shuhendler, T. Kurosawa, Y. Zhou, S. Gambhir, Z. Bao and J. Rao, *Adv. Mater.*, 2015, **27**, 5184; (*b*) Q. Zhao and J. Sun, *J. Mater. Chem. C*, 2016, **4**, 10588; (*c*) X. Liu, Z. Yang, W. Xu, Y. Chu, J. Yang, Y. Yan, Y. Hu, Y. Wang and J. Hua, *J. Mater. Chem. C*, 2019, **7**, 12509.

12 (*a*) H. Zhu, Y. Fang, Q. Miao, X. Qi, D. Ding, P. Chen and K. Pu, *ACS Nano*, 2017, **11**, 8998; (*b*) W. Wu, D. Mao, F. Hu, S. Xu, C. Chen, C. Zhang, X. Cheng, Y. Yuan, D. Ding, D. Kong and B. Liu, *Adv. Mater.*, 2017, **29**, 1700548; (*c*) L. Li, C. Shao, T. Liu, Z. Chao, H. Chen, F. Xiao, H. He, Z. Wei, Y. Zhu, H. Wang, X. Zhang, Y. Wen, B. Yang, F. He and L. Tian, *Adv. Mater.*, 2020, **32**, 2003471.

13 (*a*) J. Yamada and T. Sugimoto, *TTF Chemistry: Fundamentals & applications of Tetrathiafulvalene*, Springer Verlag, Berlin, 2004; (*b*) M. Bendikov, F. Wudl and D. Perepichka, *Chem. Rev.*, 2004, **104**, 4891; (*c*) T. Mori, *Chem. Rev.*, 2004, **104**, 4947.

14 (*a*) F. Wudl, D. Wobschall and E. J. Hufnagel, *J. Am. Chem. Soc.*, 1972, **94**, 670; (*b*) L. B. Coleman, M. J. Cohen, D. J. Sandman, F. G. Yamagishi, A. F. Garito and A. J. Heeger, *Solid State Commun.*, 1973, **12**, 1125.

15 (*a*) M. Bryce, *J. Mater. Chem.*, 2000, **10**, 589; (*b*) N. Martín and J. Segura, *Angew. Chem., Int. Ed.*, 2001, **40**, 1372; (*c*) M. Nielsen, C. Lomholt and J. Becher, *Chem. Soc. Rev.*, 2000, **29**, 153; (*d*) T. Jørgensen, T. Hansen and J. Becher, *Chem. Soc. Rev.*, 1994, **23**, 41–51.

16 (*a*) D. Canevet, M. Sallé, G. Zhang, D. Zhang and D. Zhu, *Chem. Commun.*, 2009, 2245; (*b*) A. Jana, S. Bähring, M. Ishida, S. Goeb, D. Canevet, M. Sallé, J. Jeppesen and J. Sessler, *Chem. Soc. Rev.*, 2018, **47**, 5614; (*c*) A. Jana, M. Ishida, J. Park, S. Bahring, J. Jeppesen and J. Sessler, *Chem. Rev.*, 2017, **117**, 2641.

17 C. Rovira, *Chem. Rev.*, 2004, **104**, 5289.

18 N. Duvva, U. Chilakamarthi and L. Giribabu, *Sustainable Energy Fuels*, 2017, **1**, 678.

19 (*a*) J. Spruell, A. Coskun, D. Friedman, R. Forgan, A. Sarjeant, A. Trabolsi, A. Fahrenbach, G. Barin, W. Paxton, S. Dey, M. Olson, D. Benítez, E. Tkatchouk, M. Colvin, R. Carmielli, S. Caldwell, G. Rosair, S. Hewage, F. Duclairoir, J. Seymour, A. Slawin, W. Goddard III, M. Wasielewski, G. Cooke and J. F. Stoddart, *Nat. Chem.*, 2010, **2**, 870; (*b*) J. Xiao, Z. Yin, H. Li, Q. Zhang, F. Boey, H. Zhang and Q. Zhang, *J. Am. Chem. Soc.*, 2010, **132**, 6926.

20 (*a*) X. Li, G. Zhang, H. Ma, D. Zhang, J. Li and D. Zhu, *J. Am. Chem. Soc.*, 2004, **126**, 11543; (*b*) G. Zhang, D. Zhang, X. Guo and D. Zhu, *Org. Lett.*, 2004, **6**, 1209; (*c*) H. Wu, D. Zhang, L. Su, K. Ohkubo, C. Zhang, S. Yin, L. Mao, Z. Shuai, S. Fukuzumi and D. Zhu, *J. Am. Chem. Soc.*, 2007, **129**, 6839.

21 (*a*) S. Bivaud, S. Goeb, V. Croué, P. I. Dron, M. Allain and M. Sallé, *J. Am. Chem. Soc.*, 2013, **135**, 10018; (*b*) S. Bivaud, J. Y. Balandier, M. Chas, M. Allain, S. Goeb and M. Sallé, *J. Am. Chem. Soc.*, 2012, **134**, 11968; (*c*) S. Krykun, M. Dekhtiarenko, D. Canevet, V. Carré, F. Aubriet, E. Levillain, M. Allain, Z. Voitenko, M. Sallé and S. Goeb, *Angew. Chem., Int. Ed.*, 2020, **59**, 716.

22 (*a*) C. Wang, D. Zhang and D. Zhu, *J. Am. Chem. Soc.*, 2005, **127**, 16372; (*b*) T. Kitamura, S. Nakaso, N. Mizoshita, Y. Tochigi, T. Shimomura, M. Moriyama, K. Ito and T. Kato, *J. Am. Chem. Soc.*, 2005, **127**, 14769; (*c*) T. Kitahara, M. Shirakawa, S. I. Kawano, U. Beginn, N. Fujita and S. Shinkai, *J. Am. Chem. Soc.*, 2005, **127**, 14980; (*d*) C. Wang, Q. Chen, F. Sun, D. Zhang, G. Zhang, Y. Huang, R. Zhao and D. Zhu, *J. Am. Chem. Soc.*, 2010, **132**, 3092.

23 J. Bergkamp, S. Decurtins and S. Liu, *Chem. Soc. Rev.*, 2015, **44**, 863.

24 (*a*) X. Gao, Y. Wang, X. Yang, Y. Liu, W. Qiu, W. Wu, H. Zhang, T. Qi, Y. Liu, K. Lu, C. Du, Z. Shuai, G. Yu and D. Zhu, *Adv. Mater.*, 2007, **19**, 3037; (*b*) Y. Hu, Z. Wang, X. Zhang, X. Yang, C. Ge, L. Fu and X. Gao, *Org. Lett.*, 2017, **19**, 468.

25 (*a*) G. Yang, C. Di, G. Zhang, J. Zhang, J. Xiang, D. Zhang and D. Zhu, *Adv. Funct. Mater.*, 2013, **23**, 1671; (*b*) L. Tan, Y. Guo, Y. Yang, G. Zhang, D. Zhang, G. Yu, W. Xu and Y. Liu, *Chem. Sci.*, 2012, **3**, 2530.

26 (*a*) H. Yamada, M. Yamashita, H. Hayashi, M. Suzuki and N. Aratani, *Chem. – Eur. J.*, 2018, **24**, 18601; (*b*) N. Tucker, A. Briseno, O. Acton, H. Yip, H. Ma, S. Jenekhe, Y. Xia and A. Jen, *ACS Appl. Mater. Interfaces*, 2013, **5**, 2320;

This journal is © The Royal Society of Chemistry 2022

J. Mater. Chem. C, 2022, **10**, 2814–2820 | **2819**

(*c*) M. Yamashita, K. Kawano, A. Matsumoto, N. Aratani, H. Hayashi, M. Suzuki, L. Zhang, A. Briseno and H. Yamada, *Chem. – Eur. J.*, 2017, **23**, 15002.

27 (*a*) C. Jia, S. Liu, C. Tanner, C. Leiggener, A. Neels, L. Sanguinet, E. Levillain, S. Leutwyler, A. Hauser and S. Decurtins, *Chem. – Eur. J.*, 2007, **13**, 3804; (*b*) Y. Geng, R. Pfattner, A. Campos, J. Hauser, V. Laukhin, J. Puigdollers, J. Veciana, M. Mas-Torrent, C. Rovira, S. Decurtins and S. Liu, *Chem. – Eur. J.*, 2014, **20**, 7136; (*c*) H. Jia, J. Ding, Y. Ran, S. Liu, C. Blum, I. Petkova, A. Hauser and S. Decurtins, *Chem. – Asian J.*, 2011, **6**, 3312.

28 (*a*) X. Lu, J. Sun, Y. Liu, J. Shao, L. Ma, S. Zhang, J. Zhao, Y. Shao, H. Zhang, Z. Wang and X. Shao, *Chem. – Eur. J.*, 2014, **20**, 9650; (*b*) L. Liu, C. Yan, Y. Li, Z. Liu, C. Yuan, H. Zhang and X. Shao, *Chem. – Eur. J.*, 2019, **26**, 7083; (*c*) C. Jia, J. Zhang, J. Bai, L. Zhang, Z. Wan and X. Yao, *Dyes Pigm.*, 2012, **94**, 403.

29 S. Keshri, D. Asthana, S. Chorol, Y. Kumar and P. Mukhopadhyay, *Chem. – Eur. J.*, 2018, **24**, 1821.

30 Y. Niu, Q. Peng, C. Deng, X. Gao and Z. Shuai, *J. Phys. Chem. A*, 2010, **114**, 7817.

31 Electron transport for the OFET devices with thin films of NDITTF2 was not observed even under a N_2 atmosphere or vacuum. This may be due to the fact that the LUMO of NDITTF2 is almost concentrated on the NDI moiety, while the HOMO is delocalized over TTF and the naphthalene ring of NDI. Thus, the conduction channel for electron transport cannot be formed efficiently.